forests

MDPI

Article

Estimation of Aboveground Vegetation Water Storage in Natural Forests in Jiuzhaigou National Nature Reserve of China Using Machine Learning and the Combination of Landsat 8 and Sentinel-2 Data

Xiangshan Zhou [1,2], Wunian Yang [1,*], Ke Luo [1] and Xiaolu Tang [3,4]

[1] College of Earth Science, Chengdu University of Technology, Chengdu 610059, China; zhouxiangshan@stu.cdut.edu.cn (X.Z.); luoke1997.8@gmail.com (K.L.)
[2] POWERCHINA Chengdu Engineering Corporation Limited, Chengdu 611130, China
[3] College of Ecology and Environment, Chengdu University of Technology, Chengdu 610059, China; tangxiaolu17@cdut.edu.cn
[4] State Environmental Protection Key Laboratory of Synergetic Control and Joint Remediation for Soil & Water Pollution, Chengdu University of Technology, Chengdu 610059, China
* Correspondence: ywn@cdut.edu.cn

Abstract: Aboveground vegetation water storage (AVWS) is a fundamental ecological parameter of terrestrial ecosystems which participates in plant metabolism, nutrient and sugar transport, and maintains the integrity of the hydraulic system of the plant. The Jiuzhaigou National Nature Reserve (JNNR) is located in the Eastern Tibet Plateau and it is very sensitive to climate change. However, a regional estimate of the AVWS based on observations is still lacking in the JNNR and improving the model accuracy in such mountainous areas is challenging. Therefore, in this study, we combined the Landsat 8 and Sentinel-2 data to estimate AVWS using multivariate adaptive regression splines (MARS), random forest (RF) and extreme gradient boosting (XGBoost) with the linkage of 54 field observations in the JNNR. The results showed that AVWS varied among different forest types. The coniferous forests had the highest AVWS (212.29 $\pm$ 84.43 Mg ha^{-1}), followed by mixed forests (166.29 $\pm$ 72.73 Mg ha^{-1}) and broadleaf forests (142.60 $\pm$ 46.36 Mg ha^{-1}). The average AVWS was 171.2 Mg ha^{-1}. Regardless of the modelling approaches, both Sentinel-2 and Landsat 8 successfully estimated AVWS separately. Prediction accuracy of AVWS was improved by combining Landsat 8 and Sentinel-2 images. Among the three machine learning approaches, the XGBoost model performed best with a model efficiency of 0.57 and root mean square error of 48 Mg ha^{-1}. Predicted AVWS using XGBoost showed a strong spatial pattern of across the study area. The total AVWS was 5.24 $\times$ 10^6 Mg with 67.2% coming from conifer forests. The results highlight the potential of improving the accuracy of AVWS estimation by integrating different optical images and using machine learning approaches in mountainous areas.

Keywords: machine learning; aboveground vegetation water storage; Sentinel-2; natural forests; China

Citation: Zhou, X.; Yang, W.; Luo, K.; Tang, X. Estimation of Aboveground Vegetation Water Storage in Natural Forests in Jiuzhaigou National Nature Reserve of China Using Machine Learning and the Combination of Landsat 8 and Sentinel-2 Data. *Forests* **2022**, *13*, 507. https://doi.org/10.3390/f13040507

Academic Editor: Karol Bronisz

Received: 20 February 2022
Accepted: 22 March 2022
Published: 25 March 2022

1. Introduction

Forest ecosystem accounts for about 33% of the Earth's land surface area. It is an important gene, carbon and energy pool, and water reservoir [1]. It is also a key factor to regulate the water cycle of terrestrial ecosystems [2,3]. Aboveground vegetation water storage (AVWS) is defined as the water storage of the vegetation leaves, stems and branches, which is the composition of the eco-water proposed by Wan and Yang [4]. Vegetation water storage impacts the plant metabolism, nutrient and sugar transport, and maintains the integrity of the hydraulic system of the plant [5]. Using remote sensing to estimate the AVWS at different scales is very important for estimating the water conservation function

of forest vegetation, the change of river runoff and frequent extreme weather events caused by global climate change [6–9].

Previous studies on vegetation water content mainly focused on several main indicators, such as the relative water content (RWC), relative drought index (RDI), fuel moisture content (FMC) and equivalent water thickness (EWT) [5]. Among these studies, remote sensing was commonly used for estimating the vegetation water content [8,10]. For example, Neinavaz and Skidmore [10] used thermal hyperspectral (TIR, 8–14 μm) measurements to retrieve FMC and EWT at canopy level, obtaining a good model performance. However, as an important indicator of the vegetation water content, there are few studies on the forest water storage capacity measurement due to the lack of stem water storage capacity [11].

In the last decades, remote sensing was proved to be a useful tool to estimate the vegetation water content across different scales [12,13]. Among the different sensors, Landsat 8 (Operational Land Imager), as a medium-resolution sensor (30 m), was widely used in land use classification and for the direct estimation of some surface parameters [14,15]. Compared with Landsat 8, Sentinel-2 has been shown to have unique advantages for measuring forest canopy cover, leaf area index (LAI) and aboveground biomass (AGB), due to its higher resolution (10 m) and more spectral bands (red-edge bands) [16–18]. However, whether the combination of different optical images can estimate AVWS accurately has not been studied. Thus, the potential of optical images in AVWS estimation is still to be explored, particularly in mountainous regions.

Previous studies commonly used statistical and physical models to estimate the vegetation water content based on remote sensing [19]. The traditional empirical model is represented by linear and nonlinear models, which establishes the relationships between vegetation water content indicators and vegetation indices (VIs) conducted by the bands focused on the visible, near-infrared and shortwave-infrared regions [10,20–22]. However, it is difficult to solve the saturation problem that occurs when estimating vegetation-related indicators [23]. Additionally, it has the disadvantage of creating models that may be highly dependent on location, sampling conditions and time [24,25]. Radiative transfer models (RTM) are also widely used in the estimation of vegetation water content, including PROSAIL, GeoSAIL and 4SAIL2 [26]. Many studies have accurately estimated the water storage on leaf and canopy level using RTMs [27–29]. For example, Wang and Hunt [27] using PROSPECT and SAIL model to estimate the Fuel moisture content (FMC) for single leaves and leaf stacks of *Quercus* alba, *Acer* rubrum and *Zea* mays, which obtained a good result (for the PROSPECT model simulations, the relationship between FMC and NDII/NDMI had an R^2 of 0.853, while for the SAIL model simulations, the relationship between NDII/NDMI and FMC at the canopy scale had an R^2 of 0.900). However, ill-posed model inversion complicates the use of RTMs. In addition, the influence of dry matter content on the model cannot be eliminated [30–32].

As nonparametric methods, the machine learning algorithms, such as random forest (RF), extreme gradient boosting (XGBoost) and multivariate adaptive regression splines (MARS), have been widely used for the estimation of surface parameters, e.g., AGB and LAI [33,34]. Compared with the traditional empirical model, machine learning approaches can handle a larger number of variables and describe the relationships between AVWS and variables more accurately, and it can overcome the overfitting and autocorrelation problem [35]. In addition, the machine learning algorithms required no initial assumptions about functional relationships and can function with nonlinear dependencies, which are completely data adaptive [36]. While compared with radiative transfer models, the advantage of machine learning algorithm is not reflected in accuracy, but in overcoming some defects of radiative transfer models (e.g., negative influences of dry mater content (Cm) on radiative transfer models cannot be eliminated and a few variables in radiative transfer model are difficult to measure) [30–32].

In this study, the performance of the AVWS estimation combining Sentinel-2 and Landsat 8 using machine learning approaches in the Jiuzhaigou National Nature Reserve (JNNR) was validated. The JNNR located in the Eastern Tibet Plateau, and it is a world-

famous tourist attraction, which is sensitive to global climate change [37]. The JNNR has rich primary or second forest sources, which cover more than 70% of the area [38]. An accurate estimation of AVWS in subalpine forests in the JNNR is a challenge due to the complex terrain conditions, e.g., steep slopes and varying soil depths with an elevation ranging from 1996 to 4764 m above sea level [37]. Currently, the existing studies in the JNNR mainly focused on earthquake landslide hazard assessments, post-earthquake vegetation restoration and wildlife protection [39–41]. However, to our best knowledge, a regional estimation of AVWS in the JNNR has not been carried out.

To fill the knowledge gaps, we combined the Landsat 8 and Sentinel-2 data to estimate AVWS using MARS, RF and XGBoost with the linkage of 54 field observations in the JNNR. The specific objectives of the study were to: (1) compare the AVWS among different forest types; (2) optimize the methodology to model AVWS with Landsat 8 and Sentinel-2 images using three approaches.

2. Materials and Methods

2.1. Study Area

The study area is located at the Jiuzhaigou National Nature Reserve (JNNR, 33°02′−33°21′ N, 108°38′−104°03′ E), at the southern region of the Jiuzhaigou County (Figure 1), which has an area of 65042.56 ha. The elevation of the study area is generally high in the south and low in the north. The landform is dominated by high mountains, with the altitude ranging from 1600 to 4800 m. This area has a plateau humid climate, with annual average temperature of 6–14 °C and annual precipitation of 600–840 mm. The JNNR is the second largest forest area in the Sichuan province, with a forest coverage of about 70% and a variety of protected plants such as *Larix mastersiana* Rehd. et Wils., *Taxus chinensis* (Pilger) Rehd., *Tetracentron sinense* Oliv., *Picea brachytyla* (Franch.) Pritz., *Cupressus chengiana* S. Y. Hu, *Magnolia officinalis* Rehd. et Wils., *Pteroceltis tatarinowii* Maxim. and *Picea aurantiaca* Mast.

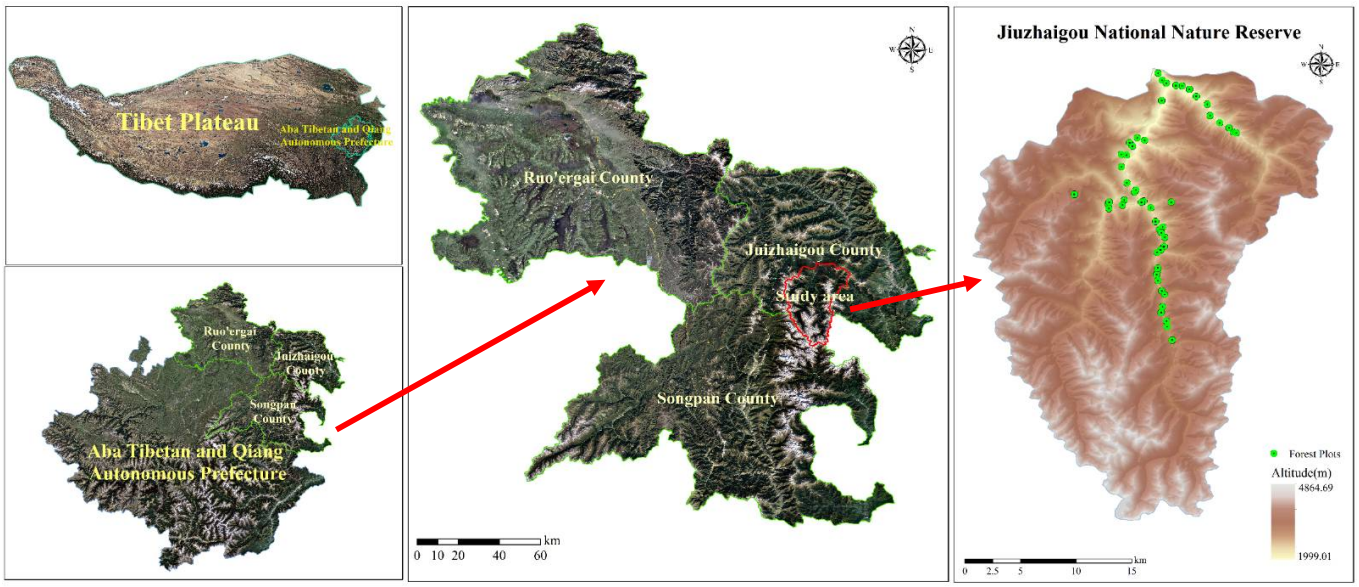

Figure 1. Location of the study area (Jiuzhaigou National Nature Reserve) and field data.

2.2. Field Data

2.2.1. Data Acquisition

Circular plots with a radius of 10 m were established from 19 June 2019 to 7 July 2019. All the sample plots were selected to be at least 100 m away from the road to reduce the edge effect [42,43]. Within each plot, all trees with a diameter greater than 5 cm at breast height (DBH) of 1.3 m were measured by a diameter tape, and the tree species was identified. Longitude, latitude, altitude and other geographic information were also

recorded. A total of 54 forest plots were collected, with an elevation from 2199 m to 3522 m, including 14 coniferous forests plots, 16 broad-leaved forests plots and 24 mixed forests plots. The total number of samples was 2938 trees, and the average stand density was 1720 trees per ha. Samples were collected for different tree species, and the fresh weight (FW) was weighted in the field. Then the samples were dried at 70 °C until a constant weight was achieved in order to calculate the water content (ω) of each tree organ.

2.2.2. Aboveground Vegetation Water Storage Calculation

Initially, the aboveground biomass, which are expressed as the dry weight (*DW*) and the fresh weight (*FW*), was calculated using the allometric equation for each organ (Table S1). Then, the AVWS of branch, leaf and stem was calculated according to Equation (1):

$$\omega = \frac{FW - DW}{FW} \times 100\% \quad (1)$$

where ω is the water content (%). According to the relationship between water content and biomass (*BM*), which is calculated according to the allometric growth equation of trees, the AVWS of branches, stems and leaves of trees can be calculated by Equation (2):

$$\text{AVWS} = \frac{\omega}{1 - \omega} \times BM \quad (2)$$

One-way analysis of variance (ANOVA) and Tukey-HSD (honestly significant difference) test were used to compare the differences of AVWS among different forest types.

2.3. Satellite Data and Preprocessing

The Sentinel-2 satellite (Table S2) carries a multispectral instrument (MSI) at a height of 786 km, covering 13 spectral bands ranged from 0.4 to 2.4 μm, at three spatial resolutions (10, 20 and 60 m), with a temporal resolution of 10 days and a width of 290 km. Among the optical data, Sentinel-2 data is the only one that contains three bands in the red edge range, which is very effective for monitoring vegetation health information. The Sentinel-2 image on 31 December 2019 was used in this study (https://scihub.copernicus.eu/dhus/odata/v1/Products('59961b5d-603c-4416-b9f5-b3e2207350b0')/value, accessed on 20 February 2022).

Landsat 8 (Table S3) was launched in 2013 by NASA, America's space agency. The satellite is equipped with two sensors, the Operational Land Imager (OLI) and the Thermal Infrared Sensor (TIRS). OLI was used to collect image data of nine short-wave spectral bands with a width of 185 km, ranged from 0.43 to 2.3 μm, at a spatial resolution of 30 m, except for band 8 (15 m). The Landsat 8 image on 22 November 2019 was used in this study (https://dds.cr.usgs.gov/download-staging/eyJpZCI6MTQ1MDU3ODczLCJjb250YWN0SWQiOjIxMTY0NjF9, accessed on 20 February 2022).

The preprocessing of the Sentinel-2 and Landsat 8 data was carried out in the Sen2Cor and ENVI 5.3 software, respectively. The main preprocessing processes include radiometric calibration, atmospheric correction, terrain correction, geometric correction and resampling. Radiometric calibration converts image DN value into TOA reflectance, and atmospheric calibration converts TOA reflectance into surface reflectance. Terrain correction and geometric correction eliminated the errors caused by the terrain fluctuation and image distortion. Finally, the Sentinel-2 image resolution was resampled to the same spatial resolution of Landsat 8 of 30 m by the bilinear approach. After the preprocessing, bands 1 to 7 and 9 of Landsat 8 and bands 1 to 13, except 10, of Sentinel-2 image were extracted as the potential predictors of AVWS. The workflow is shown in Figure 2.

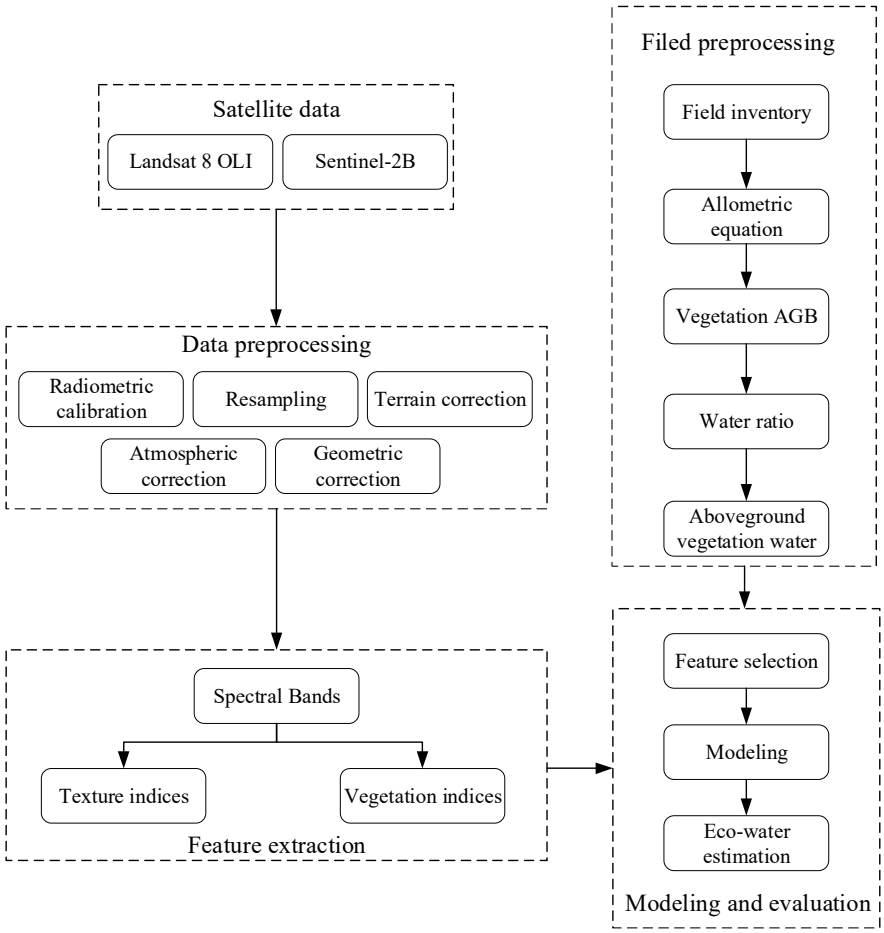

Figure 2. Workflow of the AVWS (aboveground vegetation water storage) estimation model.

There were many clouds in the study area, so it was difficult to obtain available multi-issue images at the same time. Therefore, like many previous studies [17,44], we used single-issue images to predict AVWS, and applied ten-fold cross-validation to evaluate model performance.

2.4. Classification Method

We used Sentinel-2 images and field observations for classification, with an image resolution of 10 m. The support vector machine (SVM) was applied for supervised classification using the original bands of Sentinel-2. Specifically, a total of 256 polygons (including 577 points) were used for training samples and field observations were used for test samples for an accuracy assessment. Through visual interpretation combined with the recorded vegetation types and corresponding longitude and latitude coordinates during field inventory, it was determined that the main types were forest and non-forest, in which the forest types were divided into coniferous forests, broad-leaved forests and mixed forests. After the supervised classification of the images, some small patches inevitably appeared in the results. Whether from the perspective of thematic mapping or from the perspective of practical application, it was necessary to eliminate or reclassify these small patches, so they needed to be processed by major/minority analysis, cluster and sieve.

In the major/minor analysis, the false pixels in the larger category were classified into this category by a method similar to convolution filtering, and a transform kernel size was defined. Clump processing was used to cluster and merge adjacent similar classification regions by using mathematical morphology operators (corrosion and expansion). Sieve processing solved the island problem in classified images. The filtering process used the speckle grouping method to eliminate these isolated classified pixels. The post classification

image processing was conducted through analysis tools such as "majority/minority", "clump classes" and "sieve classes" in ENVI software, and set parameters to obtain the final vegetation classification, which included "kernel size" (3*3 by default), "center pixel weight" (1 by default), "operator size rows" (3 by default), "cols" (3 by default), "group min threshold" (5 by default) and "number of neighbors" (8 by default). After the above processing, the problems of spots, holes and drum islands in the classified image were solved, and the spatial continuity and smoothness of the image were enhanced (Figure S1, Table S4).

In this study, the classification results were evaluated by overall accuracy (OA) and kappa coefficient. Overall accuracy (OA) refers to the ratio of the number of correctly classified category pixels to the total number of categories [45]:

$$\mathrm{OA} = \frac{n}{N} \tag{3}$$

where n is the number of all correctly classified units, and N is the number of all classified units.

Kappa coefficient (Kappa) is a proportion, which represents the proportion of error reduction between classification and completely random classification [45], calculated by Equation (4):

$$K = \frac{p_0 - p_e}{1 - p_e} \tag{4}$$

where p_0 is the overall accuracy, and p_e can be calculated by Equation (5):

$$p_e = \frac{a_1 \times b_1 + a_2 \times b_2 + \cdots + a_c \times b_c}{n \times n} \tag{5}$$

where $a_1, a_2 \ldots a_c$ is the number of real samples of each class, and $b_1, b_2 \ldots b_c$ is the number of samples of each class predicted, and n is the total number of samples.

2.5. Variables for the Prediction of Aboveground Vegetation Water Storage

According to typical spectral characteristics of vegetation, such as reflectance peaks, absorption bands and red edges, we also extracted the following indices (Table S5): Perpendicular Vegetation Index (PVI) [46], Triangle Vegetation Index (TVI) [47], Difference Vegetation Index (DVI) [48], Normalized Green–Blue Difference Index (NGBDI) [49], Green–Blue Ratio Index (GBRI) [50], Atmospherically Resistant Vegetation Index (ARVI) [51], Green–Red Ratio Index (GRRI) [52], Specific Leaf Area Vegetation Index (SLAVI) [53], Normalized Different Moisture Index (NDMI) [54] and Normalized Difference Infrared Index (NDII) [55].

Texture is a feature representing the correlation between pixels in a region, which can be used for the classification of images and to provide information related to the structure and geometric properties of forests [56,57]. In this study, we used the gray level co-occurrence matrix texture analysis method proposed by Haralick [58] to calculate eight common texture features derived from Sentinel-2 and Landsat 8 with a 5 × 5 window size, which included mean, variance, homogeneity, contrast, dissimilarity, entropy, second moment and correlation (Table S6).

2.6. Feature Selection

We used Pearson's correlation to analyze the relationships between field AVWS and the above variables listed based on the image after resampling the Sentinel-2 image to 30 m resolution and Landsat 8 images. The variables with significant correlations ($p < 0.05$) were selected. Finally, a total of 60 variables were retained, including: (1) 26 Sentinel-2 variables; (2) 34 Landsat 8 variables; and (3) their combination (60 predictors) (Figure S2).

Then, we used the recursive feature elimination (RFE) to select the most important variables from the 60 variables to build the model. The RFE algorithm was used to evaluate the impact of the number of input features on the performance of the model. The feature

selection process started from all the indicators of each data set and ranked the predictor indicators according to the importance criteria of each regression method. Then, the less important variables were removed, until there were two predictors left. Finally, the optimal feature subset size was obtained, which was defined as the minimum prediction number within the 95% confidence interval of the minimum *RMSE*. In this study, the remaining number of variables is shown in Table S7 and the rank of the variables′ importance is shown in Figure S3.

2.7. Models

2.7.1. XGBoost

The XGBoost algorithm is proposed by Chen and Guestrin [59]. It is a flexible and highly scalable tree structure enhancement model. It can deal with sparse data, greatly improve the speed of the algorithm and reduce the computational memory in very large-scale data training. Compared with the general gradient boost method, XGBoost performs the second-order Taylor expansion of the objective function, and uses the second-order derivative in the training process to accelerate the convergence speed of the model [60]. A regularization term is added to the objective function to control the complexity of the tree, which could obtain a simpler model and avoid over fitting [61]. Currently, it is widely used by data scientists and provides the most advanced screening results for many problems.

2.7.2. MARS

MARS is a data analysis method proposed by Friedman [62]. The method takes the tensor product of the spline function as the basis function, which is divided into three steps: forward process, backward pruning and model selection. MARS uses a series of linear regressions to continuously learn different segments within the range of the transformed new variables, which could obtain the fitting of the whole set of data. In other words, MARS describes the nonlinear response relationship between species and environmental variables by using a series of linear segments with different slopes. It has the advantage that it can process large amounts of data with high dimensions within a short time and at high accuracy [63,64].

2.7.3. Random Forest

RF is an algorithm that integrates multiple decision trees through the idea of ensemble learning, which is proposed by Breiman [65]. Its basic unit is the decision tree, which can be regarded as the integration of several decision trees. Its working principle is to generate multiple classifiers or models to learn and predict independently [66]. For the classification problem, the output of RF adopts the majority voting method, while for the regression problem, the average value of the output of a single tree is calculated. It can monitor the internal estimation error, classification ability and correlation and determine the number of selected features [67].

2.7.4. Model Assessment

In this study, a 10-fold cross validation (CV) was used to evaluate the model performance. The 10-fold CV divided the data set into 10 subsets which contained almost the same number of samples and took one of the 10 subsets in each turn as the test set. The remaining nine subsets were used as training sets to predict the targeted value. Such process was conducted ten times for each part of the observations. Root mean square (*RMSE*) and r-squared (R^2), calculated by Equations (6) and (7), were used as the criteria to evaluate the model performance.

$$RMSE = \sqrt{\frac{\sum_{i=1}^{n}(y_i - \hat{y}_i)^2}{n}} \quad (6)$$

$$R^2 = \frac{\sum_{i=1}^{n} (\hat{y}_i - \overline{y})^2}{\sum_{i=1}^{n} (y_i - \overline{y})^2} \quad (7)$$

where $\hat{y}_i$ and y_i are the predicted AVWS and observed AVWS for the i th plot, respectively; n represents the total plots number of validations and $\overline{y}$ is the observed mean value.

3. Results

3.1. Classification

Regarding to forest and non-forest, the kappa coefficient was 0.89 and overall accuracy was 93.2%, showing a good classification. Similarly, regarding all land cover types, the overall accuracy was 84.48% and the kappa coefficient was 0.80 (Figure S1). Coniferous forests occupied the largest area (1.87×10^4 ha, 28.70%), followed by snow (1.76×10^4 ha, 27.12%), bare land (1.17×10^4 ha, 18.01%) and broadleaved forests (1.04×10^4 ha, 15.93%). Grassland, shrubland, mixed forests and waterbodies accounted for a small proportion of all land areas.

3.2. Field AVWS

The AVWS ranged from 64.06 to 443.51 Mg ha^{-1} with an average of 171.2 Mg ha^{-1} (Table 1). ANOVA analysis showed that the forest type had a significant impact on AVWS (p = 0.03). The highest AVWS was observed in coniferous forests (212.29 ± 84.43 Mg ha^{-1}), followed by mixed forests (166.29 ± 72.73 Mg ha^{-1}) and broad-leaved forests (142.60 ± 46.36 Mg ha^{-1}). From the results of the Tukey-HSD test, the difference between coniferous forests and broad-leaved forests was significant (p = 0.02), while the AVWS of coniferous forests (p = 0.13) and broad-leaved forests (p = 0.55) were not significantly different from mixed forests.

Table 1. Statistics of aboveground vegetation water storage (AVWS) of different forest types in 54 sample plots.

Vegetation Type	Average Value (Mg ha^{-1})	Standard Deviation (Mg ha^{-1})	Maximum Value (Mg ha^{-1})	Minimum Value (Mg ha^{-1})
Coniferous forest	212.29 a	84.43	443.51	89.58
Broad-leaved forest	142.6 b	46.36	245.31	82.74
Mixed forests	166.29 ab	72.73	353.21	64.06
All forests	171.2	73.19	443.51	64.06

Note: Different lowercase letters (a and b) indicate statistical significance at $p < 0.05$ using one-way analysis of variance (ANOVA) and Tukey-HSD test for multiple comparisons.

3.3. Model Comparison

After feature selection, we obtained nine models of RF, MARS and XGBoost using different data sources (Figure 3).

Regarding satellite images, the models using Sentinel-2 images generally performed better than Landsat 8 (Figure 3d–i). Additionally, the model performances were significantly improved when integrating Sentinel-2 and Landsat 8 variables (Figure 3a–c).

Among the three different modeling approaches, XGBoost performed best, followed by RF and MARS. Therefore, the XGBoost model combining Landsat 8 and Sentinel-2 images was selected for the spatial modeling of AVWS (R^2 = 0.57, $RMSE$ = 48 Mg ha^{-1}, Figure 3c).

3.4. Spatial Distribution Characteristics of AVWS

The predicted AVWS showed a strong spatial variability (Figure 4), varying from 52 to 363 Mg ha^{-1}. The total AVWS was 5.2×10^6 Mg across the study area (Table 2). Forest types had a great impact on AVWS. AVWS mainly focused on coniferous forests, followed by broad-leaved forests, shrubland and mixed forests. Spatially, high AVWS was mainly found in the North and central areas, while the AVWS in the Southern region was relatively low.

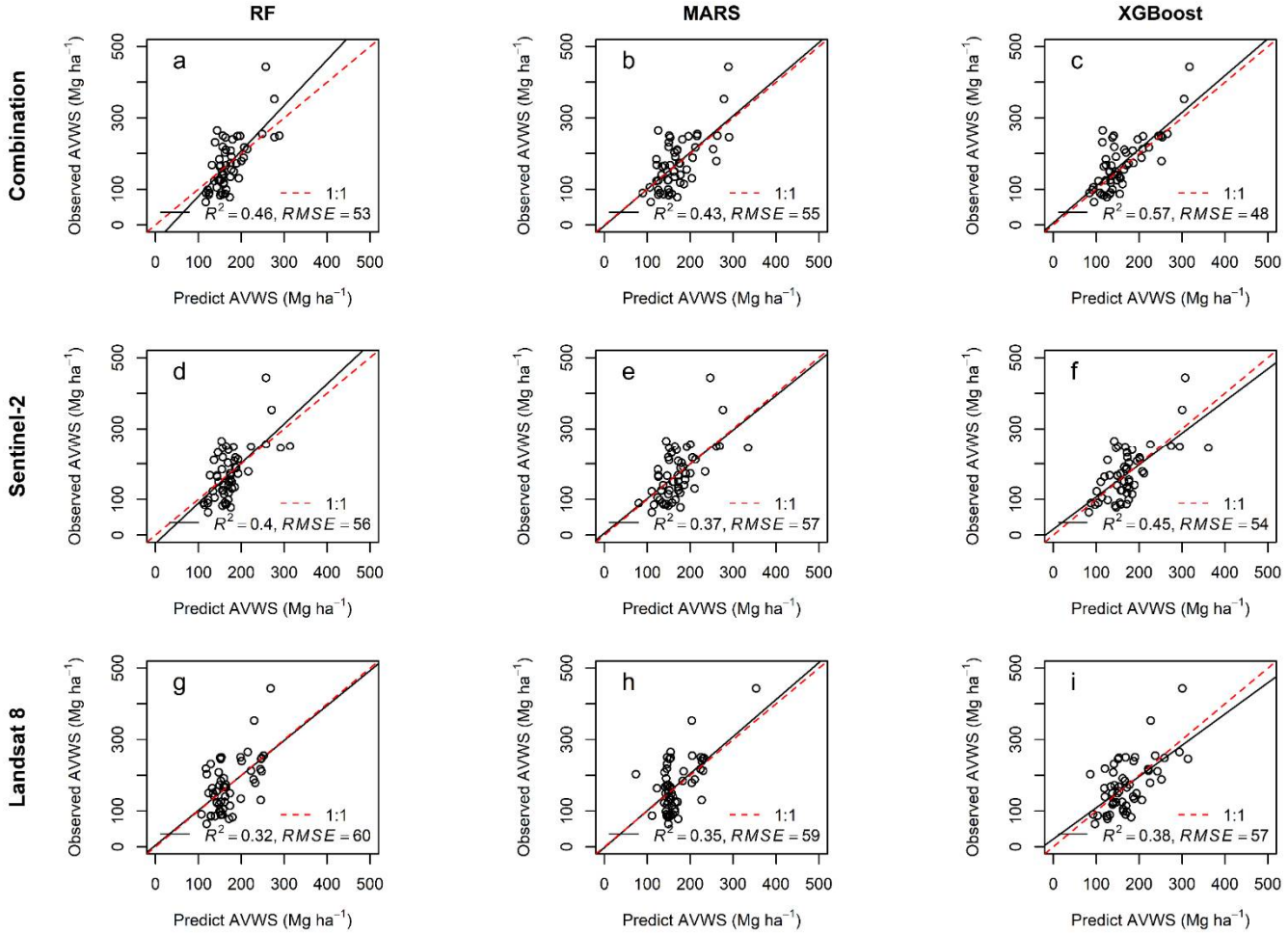

Figure 3. The correlation between predicted and observed aboveground vegetation water storage (AVWS) using different modelling approaches (XGBoost, RF and MARS) and satellite images (Landsat 8 and Sentinel-2).

Table 2. Statistics of the aboveground vegetation water storage (AVWS) in the study area.

Vegetation Types	AVWS (10^5 Mg)	Percentage
Coniferous forests	35.2	67.2%
Broad-leaved forests	13.3	25.4%
Mixed forests	1.4	2.7%
Shrubland	2.5	4.7%
Total	52.4	100%

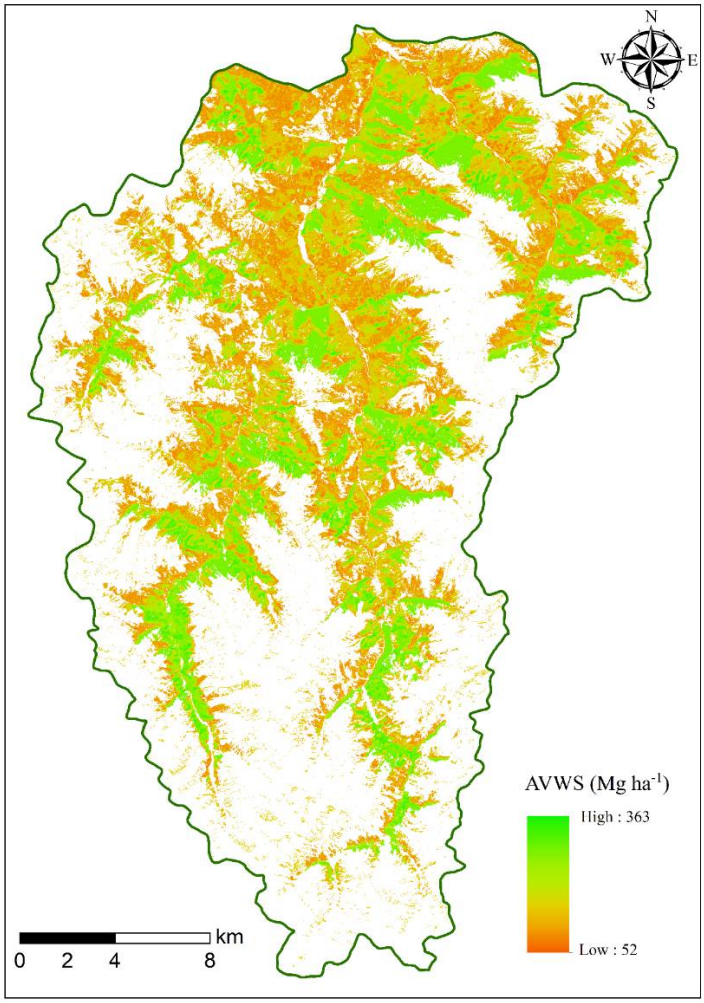

Figure 4. Modelled aboveground vegetation water storage (Mg ha^{-1}) in the Jiuzhaigou National Nature Reserve.

4. Discussion

Based on ANOVA, our results showed that differences of AVWS among forest types were significant across the study area (p = 0.03). As the JNNR belongs to a mountainous region with elevation ranging from 1600 to 4800 m, the climate is more suitable for the growth of coniferous forests, which are often taller than broad-leaved forests. The water stocked in the stem is positively correlated with wood volume and tree height [11,68]. Thus, this results in a significant difference between coniferous and broad-leaved forests.

In this study, results showed that models using Sentinel-2 outperformed those of Landsat 8 for AVWS estimation (Figure 3). This may be attributed to the higher resolution (10 m) and more spectral bands (red-edge bands) of Sentinel-2 compared with Landsat 8 [69]. Additionally, due to the saturation problem which occurs in the high vegetation cover area, using medium-resolution data such as Landsat 8 to estimate AVWS has lower accuracy, especially in complex and dense forest areas [70]. Previous studies have shown that high resolution optical remote sensing data such as Sentinel-2 and its strategic positioning band (red-edge band) may be an effective way to overcome this problem [69]. Our results also showed that integrating Landsat 8 and Sentinel-2 data greatly improved the estimation of AVWS. Different optical images have different parameters, e.g., zenith angles, azimuths and imaging times, that complement the forest information acquisition and address the problems caused by shadows, especially in mountainous regions.

Currently, statistical and physical models were commonly used to estimate AVWS [19]. However, the traditional empirical model cannot solve the saturation problem and it has

the disadvantage of creating models that may be highly dependent on location, sampling conditions and time [23–25]. In contrast, the use of RTMs is faced with the problem of ill-posed model inversion, and the influence of dry matter content on the model cannot be eliminated [30–32]. Riano and Vaughan [32] have used the PROSPECT model to estimate the fuel moisture content (FMC), which can be calculated by dividing equivalent water thickness (EWT) by dry matter content (DM), and obtained a poor result for FMC estimation when the leaf samples were fresh (R^2 = 0.33), which could be attributed to that water absorption masks the effects of DM on the spectral response. Compared with the traditional empirical model and RTMs, machine learning algorithms could overcome these defects, because they require no initial assumptions about functional relationships and can function with nonlinear dependencies, which are completely data adaptive [36]. In this study, we used three machine learning approaches to establish the models for AVWS estimation, which showed good performance. The XGBoost performed best with the highest R^2 and the lowest *RMSE*, followed by RF and MARS. The XGBoost model is a flexible algorithm, which belongs to the advanced Gradient Boosting (GB) system, and it can correct residual errors on the basis of the previous tree to generate a new tree. In contrast, the trees are independent in the RF model [59,71].

With regard to the variables selected in this study, the original bands and texture index were the most important to the AVWS model. For the original bands, the NIR and SWIR bands were more effective than the others, which may be attributed to strong reflection of vegetation in the NIR region and strong absorption caused by water in the SWIR region. It is also noted that the texture variables have an important effect on AVWS prediction, which may partially compensate some of the band saturation problem especially in forests with complex structure [72,73].

AVWS showed strong spatial patterns in the JNNR, which may be influenced by the ecosystem and elevation. Generally, vegetation growth is restricted with elevation, and AVWS in forest ecosystem are more abundant than the other ecosystem [10]. In this study, AVWS showed higher values in mountains with low altitude, which were covered with a large number of coniferous forests, broadleaf forests and mixed forests, while AVWS showed lower values in mountains with high altitude which were covered with shrubland, snow and bare soil. Meanwhile, with regards to the overall spatial distribution pattern, high AVWS was mainly found in the north and central areas, while it was relatively low in the southern region. This was contrary to the variation in elevations in the study area where the terrain was high in the south and low in the north.

Although this study obtained good results predicting AVWS, there were still some limitations. First, the inventory plots could not fully describe the characteristics of the vegetation in the JNNR. Therefore, these should be increased considering different types (coniferous forests, broad-leaved forests, mixed forests and shrubs) and a wider range of vertical distribution, especially above 3000 m. Second, due to the influence of cloud cover and satellite imaging period, the acquisition time of Landsat 8 and Sentinel-2 images was inconsistent. Third, the spatial uncertainty of AVWS in the study area was not obtained because of the uneven distribution of the forest inventory plots. However, to overcome this limitation, we set the forest inventory plots along an elevation from 2199 m to 3522 m, which could represent the majority of forest conditions across the study area. This can bias the prediction results through spectral variability. Fourth, when separating observations of different forest types to test the models, it was found that the model could only accurately predict the AVWS of coniferous forests (Figure S4) and mixed forests (Figure S5), while the prediction of broad-leaved forests AGB was poor (Figure S6). This may be attributed to the different spectral characteristics and the significantly different AVWS values of coniferous forest and broadleaved forest.

5. Conclusions

In this study, based on 54 inventory plots, we used three kinds of machine learning algorithms (XGBoost, MARS and RF) to model AVWS across the JNNR using Sentinel-2 and

Landsat 8. Robust conclusions included: (1) The AVWS varied from 64.06 to 443.51 Mg ha^{-1}, and had an average of 171.2 Mg ha^{-1}, which showed a strong spatial variability. (2) The XGBoost model performed better than MARS and RF, with an efficiency of 0.57 and root mean squared error of 48 Mg ha^{-1}. (3) Regardless of the modelling approaches, integrating Sentinel-2 and Landsat 8 improved the performance of the estimation of AVWS. This result highlighted a potential approach to improve the accuracy of AVWS estimation by integrating different optical images in mountainous areas. The outcomes of this study could provide an important scientific basis for the estimation of regional AVWS in subalpine forests, which could be used to monitor AVWS under complex terrain conditions, e.g., deep slopes.

Supplementary Materials: The following are available online at https://www.mdpi.com/article/10.3390/f13040507/s1, Figure S1: Classification of land cover in the study area, Figure S2: The correlations between AVWS and the variables of Sentinel-2B and Landsat 8 OLI. The 15 variables most correlated with AVWS were showed at a significance of $p < 0.05$, Figure S3: The Importance of variables from three dataset (Landsat 8, Sentinel-2 and their combination) using RF, XGB, and MARS algorithms, Figure S4: The correlation between predicted and observed aboveground vegetation water storage (AVWS) of coniferous forest using different modelling approaches (XGBoost, RF and MARS) and satellite images (Landsat 8 and Sentinel-2), Figure S5: The correlation between predicted and observed aboveground vegetation water storage (AVWS) of mixed forest using different modelling approaches (XGBoost, RF and MARS) and satellite images (Landsat 8 and Sentinel-2)., Figure S6: The correlation between predicted and observed aboveground vegetation water storage (AVWS) of broadleaved forest using different modelling approaches (XGBoost, RF and MARS) and satellite images (Landsat 8 and Sentinel-2), Table S1: The allometric equation of trees for estimating field AVWS [74–78], Table S2: Sentinel-2 Satellite sensor parameters, Table S3: Landsat 8 Satellite sensor parameters, Table S4: The statistics of the land cover in Jiuzhaigou National Nature Reserve, Table S5: Vegetation indices to estimate AVWS [46–55]. Table S6: Texture indices to estimate AVWS, Table S7: The number of the variables input to the model.

Author Contributions: All authors contributed to the development of ideas and analysis of output Results. Data curation, X.Z. and K.L.; Investigation, X.Z. and K.L.; Methodology, X.Z. and W.Y.; Software, X.Z. and K.L.; Supervision, W.Y. and X.T.; Writing—original draft, X.Z.; Writing—review & editing, W.Y. and X.T. All authors have read and agreed to the published version of the manuscript.

Funding: This study was primarily supported by National Natural Science Foundation of China ("Remote Sensing Dynamic Monitoring Method of Vegetation Eco-Water and Water Stress in West Sichuan Plateau"; grant number 41671432).

Institutional Review Board Statement: Not applicable.

Informed Consent Statement: Not applicable.

Data Availability Statement: The data presented in this study are available on request from the corresponding author, Wunian Yang.

Conflicts of Interest: The authors declare no conflict of interest.

References

1. FAO. *Global Forest Resources Assessment 2015*; UN Food and Agriculture Organization: Rome, Italy, 2015.
2. Qureshi, A.; Badola, R.; Hussain, S.A. A review of protocols used for assessment of carbon stock in forested landscapes. *Environ. Sci. Policy* **2012**, *16*, 81–89. [CrossRef]
3. Reichstein, M.; Carvalhais, N. Aspects of Forest Biomass in the Earth System: Its Role and Major Unknowns. *Surv. Geophys.* **2019**, *40*, 693–707. [CrossRef]
4. Wan, X.N.; Yang, W.N.; Wu, B.F. Conception of Eco-Water Sphere and Its Application. *Adv. Earth Sci.* **2004**, *19*, 117–121.
5. Gao, Z.Q.; Wang, Q.X.; Cao, X.M. The responses of vegetation water content (EWT) and assessment of drought monitoring along a coastal region using remote sensing. *Giscience Remote Sens.* **2014**, *51*, 1–16. [CrossRef]
6. Doherty, T.J.; Clayton, S. The Psychological Impacts of Global Climate Change. *Am. Psychol.* **2011**, *66*, 265–276. [CrossRef]
7. Yebra, M.; Dennison, P.E.; Chuvieco, E. A global review of remote sensing of live fuel moisture content for fire danger assessment: Moving towards operational products. *Remote Sens. Environ.* **2013**, *136*, 455–468. [CrossRef]

8. Mendiguren, G.; Martin, M.P.; Nieto, H. Seasonal variation in grass water content estimated from proximal sensing and MODIS time series in a Mediterranean Fluxnet site. *Biogeosciences* **2015**, *12*, 5523–5535. [CrossRef]
9. Quan, X.W.; He, B.B.; Li, X. A Bayesian Network-Based Method to Alleviate the Ill-Posed Inverse Problem: A Case Study on Leaf Area Index and Canopy Water Content Retrieval. *IEEE Trans. Geosci. Remote Sens.* **2015**, *53*, 6507–6517. [CrossRef]
10. Neinavaz, E.; Skidmore, A.K.; Darvishzadeh, R. Retrieving vegetation canopy water content from hyperspectral thermal measurements. *Agric. For. Meteorol.* **2017**, *247*, 365–375. [CrossRef]
11. Hunt, E.R.; Li, L.; Friedman, J.M. Incorporation of Stem Water Content into Vegetation Optical Depth for Crops and Woodlands. *Remote Sens.* **2018**, *10*, 273. [CrossRef]
12. Gao, Y.; Walker, J.P.; Allahmoradi, M. Optical Sensing of Vegetation Water Content: A Synthesis Study. *IEEE J. Sel. Top. Appl. Earth Obs. Remote Sens.* **2015**, *8*, 1456–1464. [CrossRef]
13. Zhu, X.; Skidmore, A.K.; Darvishzadeh, R. Estimation of forest leaf water content through inversion of a radiative transfer model from LiDAR and hyperspectral data. *Int. J. Appl. Earth Obs. Geoinf.* **2019**, *74*, 120–129. [CrossRef]
14. Forkuor, G.; Dimobe, K.; Serme, I. Landsat-8 vs. Sentinel-2: Examining the added value of sentinel-2's red-edge bands to land-use and land-cover mapping in Burkina Faso. *GIScience Remote Sens.* **2018**, *55*, 331–354. [CrossRef]
15. López-Serrano, P.M.; Cárdenas Domínguez, J.L.; Corral-Rivas, J.J. Modeling of Aboveground Biomass with Landsat 8 OLI and Machine Learning in Temperate Forests. *Forests* **2020**, *11*, 11. [CrossRef]
16. Korhonen, L.; Packalen, P.; Rautiainen, M. Comparison of Sentinel-2 and Landsat 8 in the estimation of boreal forest canopy cover and leaf area index. *Remote Sens. Environ.* **2017**, *195*, 259–274. [CrossRef]
17. Pandit, S.; Tsuyuki, S.; Dube, T. Estimating Above-Ground Biomass in Sub-Tropical Buffer Zone Community Forests, Nepal, Using Sentinel 2 Data. *Remote Sens.* **2018**, *10*, 601. [CrossRef]
18. Moradi, F.; Darvishsefat, A.A.; Pourrahmati, M.R. Estimating Aboveground Biomass in Dense Hyrcanian Forests by the Use of Sentinel-2 Data. *Forests* **2022**, *13*, 104. [CrossRef]
19. Zhang, J.H.; Xu, Y.; Yao, F.M. Advances in estimation methods of vegetation water content based on optical remote sensing techniques. *Sci. China-Technol. Sci.* **2010**, *53*, 1159–1167. [CrossRef]
20. Clevers, J.; Kooistra, L.; Schaepman, M.E. Estimating canopy water content using hyperspectral remote sensing data. *Int. J. Appl. Earth Obs. Geoinf.* **2010**, *12*, 119–125. [CrossRef]
21. Mirzaie, M.; Darvishzadeh, R.; Shakiba, A. Comparative analysis of different uni-and multi-variate methods for estimation of vegetation water content using hyper-spectral measurements. *Int. J. Appl. Earth Obs. Geoinf.* **2014**, *26*, 1–11. [CrossRef]
22. Ali, I.; Greifeneder, F.; Stamenkovic, J. Review of Machine Learning Approaches for Biomass and Soil Moisture Retrievals from Remote Sensing Data. *Remote Sens.* **2015**, *7*, 16398–16421. [CrossRef]
23. Ceccato, P.; Gobron, N.; Flasse, S. Designing a spectral index to estimate vegetation water content from remote sensing data: Part 1-Theoretical approach. *Remote Sens. Environ.* **2002**, *82*, 188–197. [CrossRef]
24. Cheng, T.; Rivard, B.; Sanchez-Azofeifa, A.G. Predicting leaf gravimetric water content from foliar reflectance across a range of plant species using continuous wavelet analysis. *J. Plant Physiol.* **2012**, *169*, 1134–1142. [CrossRef] [PubMed]
25. Darvishzadeh, R.; Matkan, A.A.; Ahangar, A.D. Inversion of a Radiative Transfer Model for Estimation of Rice Canopy Chlorophyll Content Using a Lookup-Table Approach. *IEEE J. Sel. Top. Appl. Earth Obs. Remote Sens.* **2012**, *5*, 1222–1230. [CrossRef]
26. Jacquemoud, S.; Baret, F. Prospect-a Model of Leaf Optical Properties Spectra. *Remote Sens. Environ.* **1990**, *34*, 75–91. [CrossRef]
27. Wang, L.L.; Hunt, E.R.; Qu, J.J. Remote sensing of fuel moisture content from ratios of narrow-band vegetation water and dry-matter indices. *Remote Sens. Environ.* **2013**, *129*, 103–110. [CrossRef]
28. Feret, J.B.; Francois, C.; Asner, G.P. PROSPECT-4 and 5: Advances in the leaf optical properties model separating photosynthetic pigments. *Remote Sens. Environ.* **2008**, *112*, 3030–3043. [CrossRef]
29. Trombetti, M.; Riano, D.; Rubio, M.A. Multi-temporal vegetation canopy water content retrieval and interpretation using artificial neural networks for the continental USA. *Remote Sens. Environ.* **2008**, *112*, 203–215. [CrossRef]
30. Combal, B.; Baret, F.; Weiss, M. Retrieval of canopy biophysical variables from bidirectional reflectance-Using prior information to solve the ill-posed inverse problem. *Remote Sens. Environ.* **2003**, *84*, 1–15. [CrossRef]
31. Koetz, B.; Baret, F.; Poilve, H. Use of coupled canopy structure dynamic and radiative transfer models to estimate biophysical canopy characteristics. *Remote Sens. Environ.* **2005**, *95*, 115–124. [CrossRef]
32. Riano, D.; Vaughan, P.; Chuvieco, E. Estimation of fuel moisture content by inversion of radiative transfer models to simulate equivalent water thickness and dry matter content: Analysis at leaf and canopy level. *IEEE Trans. Geosci. Remote Sens.* **2005**, *43*, 819–826. [CrossRef]
33. de Almeida, C.T.; Galvao, L.S.; de Oliveira Cruz e Aragao, L.E. Combining LiDAR and hyperspectral data for aboveground biomass modeling in the Brazilian Amazon using different regression algorithms. *Remote Sens. Environ.* **2019**, *232*, 111323. [CrossRef]
34. Wang, J.; Xiao, X.; Bajgain, R. Estimating leaf area index and aboveground biomass of grazing pastures using Sentinel-1, Sentinel-2 and Landsat images. *ISPRS J. Photogramm. Remote Sens.* **2019**, *154*, 189–201. [CrossRef]
35. Hanes, J. *Biophysical Applications of Satellite Remote Sensing*; Springer Science & Business Media: Berlin/Heidelberg, Germany, 2013.
36. Bodesheim, P.; Jung, M.; Gans, F. Upscaled diurnal cycles of land-atmosphere fluxes: A new global half-hourly data product. *Earth Syst. Sci. Data* **2018**, *10*, 1327–1365. [CrossRef]

37. Bossard, C.C.; Cao, Y.T.; Wang, J.Y. New patterns of establishment and growth of Picea, Abies and Betula tree species in subalpine forest gaps of Jiuzhaigou National Nature Reserve, Sichuan, southwestern China in a changing environment. *For. Ecol. Manag.* **2015**, *356*, 84–92. [CrossRef]
38. Li, W.; Ge, X.; Liu, C. Hiking trails and tourism impact assessment in protected area: Jiuzhaigou Biosphere Reserve, China. *Environ. Monit. Assess.* **2005**, *108*, 279–293. [CrossRef]
39. Zhang, Y.; Lei, K.; Zhang, Y. Effects of vegetation, elevation and human disturbance on the distribution of large-and medium-sized wildlife: A case study in Jiuzhaigou Nature Reserve. *Acta Ecol. Sin.* **2012**, *32*, 4228–4235. [CrossRef]
40. Chen, X.Q.; Chen, J.G.; Cui, P. Assessment of prospective hazards resulting from the 2017 earthquake at the world heritage site Jiuzhaigou Valley, Sichuan, China. *J. Mt. Sci.* **2018**, *15*, 779–792. [CrossRef]
41. Chen, R.; Guo, X.; Du, J. Monitoring of disturbance on ecological environment caused by earthquake and post-disaster reconstruction at heye village area of jiuzhaigou using the high-resolution remote sensing imageries. *Quat. Sci.* **2020**, *40*, 1350–1358.
42. Deljouei, A.; Sadeghi, S.M.M.; Abdi, E. The impact of road disturbance on vegetation and soil properties in a beech stand, Hyrcanian forest. *Eur. J. For. Res.* **2018**, *137*, 759–770. [CrossRef]
43. Rahbarisisakht, S.; Moayeri, M.H.; Hayati, E. Changes in Soil's Chemical and Biochemical Properties Induced by Road Geometry in the Hyrcanian Temperate Forests. *Forests* **2021**, *12*, 1805. [CrossRef]
44. Li, Y.C.; Li, M.L.; Li, C.; Liu, Z.Z. Forest Aboveground Biomass Estimation Using Landsat 8 and Sentinel-1A Data with Machine Learning Algorithms. *Sci. Rep.* **2020**, *10*, 9952. [CrossRef] [PubMed]
45. Dempster, A.P. Upper and Lower Probabilities Induced by a Multivalued Mapping. In *Classic Works of the Dempster-Shafer Theory of Belief Functions*; Yager, R.R., Liu, L., Eds.; Springer: Berlin/Heidelberg, Germany, 2008; pp. 57–72.
46. Roujean, J.L.; Breon, F.M. Estimating par absorbed by vegetation from bidirectional reflectance measurements. *Remote Sens. Environ.* **1995**, *51*, 375–384. [CrossRef]
47. Broge, N.H.; Leblanc, E. Comparing prediction power and stability of broadband and hyperspectral vegetation indices for estimation of green leaf area index and canopy chlorophyll density. *Remote Sens. Environ.* **2001**, *76*, 156–172. [CrossRef]
48. Jordan, C.F. Derivation of leaf-area index from quality of light on the forest floor. *Ecology* **1969**, *50*, 663–666. [CrossRef]
49. Hunt, E.R.; Cavigelli, M.; Daughtry, C.S.T. Evaluation of Digital Photography from Model Aircraft for Remote Sensing of Crop Biomass and Nitrogen Status. *Precis. Agric.* **2005**, *6*, 359–378. [CrossRef]
50. Sellaro, R.; Crepy, M.; Ariel Trupkin, S. Cryptochrome as a Sensor of the Blue/Green Ratio of Natural Radiation in Arabidopsis. *Plant Physiol.* **2010**, *154*, 401–409. [CrossRef]
51. Kaufman, Y.J.; Tanre, D. Atmospherically resistant vegetation index (ARVI) for EOS-MODIS. *IEEE Trans. Geosci. Remote Sens.* **1992**, *30*, 261–270. [CrossRef]
52. Rondeaux, G.; Steven, M.; Baret, F. Optimization of soil-adjusted vegetation indices. *Remote Sens. Environ.* **1996**, *55*, 95–107. [CrossRef]
53. Lymburner, L.; Beggs, P.J.; Jacobson, C.R. Estimation of canopy-average surface-specific leaf area using Landsat TM data. *Photogramm. Eng. Remote Sens.* **2000**, *66*, 183–192.
54. Hardisky, M.A.; Klemas, V.; Smart, M. The influence of soil salinity, growth form, and leaf moisture on the spectral radiance of Spartina alterniflora canopies. *Photogramm. Eng. Remote Sens.* **1983**, *49*, 77–83.
55. Hunt, E.R., Jr.; Rock, B.N. Detection of changes in leaf water content using near-and middle-infrared reflectances. *Remote Sens. Environ.* **1989**, *30*, 43–54.
56. Haralick, R.M.; Shanmugam, K.; Dinstein, I.H. Textural features for image classification. *IEEE Trans. Syst. Man Cybern.* **1973**, *3*, 610–621. [CrossRef]
57. De Grandi, G.D.; Lucas, R.M.; Kropacek, J. Analysis by Wavelet Frames of Spatial Statistics in SAR Data for Characterizing Structural Properties of Forests. *IEEE Trans. Geosci. Remote Sens.* **2009**, *47*, 494–507. [CrossRef]
58. Haralick, R.M. Statistical and structural approaches to texture. *Proc. IEEE* **1979**, *67*, 786–804. [CrossRef]
59. Chen, T.; Guestrin, C. Xgboost: A scalable tree boosting system. In Proceedings of the 22nd Acm Sigkdd International Conference on Knowledge Discovery and Data Mining, San Francisco, CA, USA, 13 August 2016; pp. 785–794.
60. He, H.; Zhang, W.; Zhang, S. A novel ensemble method for credit scoring: Adaption of different imbalance ratios. *Expert Syst. Appl.* **2018**, *98*, 105–117. [CrossRef]
61. James, G.; Witten, D.; Hastie, T. *An Introduction to Statistical Learning*; Springer: Berlin/Heidelberg, Germany, 2013.
62. Friedman, J.H. Multivariate adaptive regression splines. *Ann. Stat.* **1991**, *19*, 1–67. [CrossRef]
63. Chou, S.M.; Lee, T.S.; Shao, Y.E. Mining the breast cancer pattern using artificial neural networks and multivariate adaptive regression splines. *Expert Syst. Appl.* **2004**, *27*, 133–142. [CrossRef]
64. Balshi, M.S.; McGuirez, A.D.; Duffy, P. Assessing the response of area burned to changing climate in western boreal North America using a Multivariate Adaptive Regression Splines (MARS) approach. *Glob. Change Biol.* **2009**, *15*, 578–600. [CrossRef]
65. Breiman, L. Random forests. *Mach. Learn.* **2001**, *45*, 5–32. [CrossRef]
66. Gounaridis, D.; Koukoulas, S. Urban land cover thematic disaggregation, employing datasets from multiple sources and RandomForests modeling. *Int. J. Appl. Earth Obs. Geoinf.* **2016**, *51*, 1–10. [CrossRef]
67. Chan, J.C.W.; Paelinckx, D. Evaluation of Random Forest and Adaboost tree-based ensemble classification and spectral band selection for ecotope mapping using airborne hyperspectral imagery. *Remote Sens. Environ.* **2008**, *112*, 2999–3011. [CrossRef]

68. Nelson, R.; Short, A.; Valenti, M. Measuring biomass and carbon in delaware using an airborne profiling LIDAR. *Scand. J. For. Res.* **2005**, *20*, 283–284. [CrossRef]
69. Sibanda, M.; Mutanga, O.; Rouget, M. Examining the potential of Sentinel-2 MSI spectral resolution in quantifying above ground biomass across different fertilizer treatments. *ISPRS J. Photogramm. Remote Sens.* **2015**, *110*, 55–65. [CrossRef]
70. Adam, E.; Mutanga, O.; Rugege, D. Multispectral and hyperspectral remote sensing for identification and mapping of wetland vegetation: A review. *Wetl. Ecol. Manag.* **2010**, *18*, 281–296. [CrossRef]
71. Friedman, J.H. Stochastic gradient boosting. *Comput. Stat. Data Anal.* **2002**, *38*, 367–378. [CrossRef]
72. Li, C.; Li, Y.; Li, M. Improving Forest Aboveground Biomass (AGB) Estimation by Incorporating Crown Density and Using Landsat 8 OLI Images of a Subtropical Forest in Western Hunan in Central China. *Forests* **2019**, *10*, 104. [CrossRef]
73. Lu, D.; Batistella, M.; Moran, E. Satellite estimation of aboveground biomass and impacts of forest stand structure. *Photogramm. Eng. Remote Sens.* **2005**, *71*, 967–974. [CrossRef]
74. Shi, P.L.; Zhong, Z.C.; Li, X.G. A study on the biomass of alder and cypress artificial mixed forest in sichuan. *Acta Phytoecol. Sin.* **1996**, *20*, 524–533.
75. Kong, W.J.; Zheng, Z. The Aboveground Biomass and Net Primary Productivity of Degraded and Artificial Communities in Maoxian, Upper Reach of Minjiang River. *J. Mt. Sci.* **2004**, *22*, 445–450.
76. Luo, T.X.; Shi, P.L.; Luo, J.; Ou, Y.H. Distribution patterns of aboveground biomass in tibetan alpine vegetation transects. *Acta Phytoecol. Sin.* **2002**, *26*, 668–676.
77. Li, W.B. Study on Biomass compositions of Principal vegetations and their relationships in the Dagou Valley of the upper Minjiang River. Master's Thesis, Southwest University, Chongqing, China, 2007.
78. Luo, Y.J.; Wang, X.K.; Lu, F. *Comprehensive Database of Biomass Regressions for China's Tree Species*; China Forestry Publishing House: Beijing, China, 2015.